

# Halo-independent methods for inelastic dark matter scattering

Nassim Bozorgnia,<sup>a</sup> Juan Herrero-Garcia,<sup>b</sup> Thomas Schwetz<sup>a</sup> and Jure Zupan<sup>c</sup>

<sup>a</sup>Max-Planck-Institut für Kernphysik,  
Saupfercheckweg 1, 69117 Heidelberg, Germany

<sup>b</sup>Departamento de Física Teórica, and IFIC, Universidad de Valencia-CSIC  
Edificio de Institutos de Paterna, Apt. 22085, 46071 Valencia, Spain

<sup>c</sup>Department of Physics, University of Cincinnati,  
Cincinnati, Ohio 45221, USA

E-mail: [bozorgnia@mpi-hd.mpg.de](mailto:bozorgnia@mpi-hd.mpg.de), [juan.a.herrero@uv.es](mailto:juan.a.herrero@uv.es),  
[schwetz@mpi-hd.mpg.de](mailto:schwetz@mpi-hd.mpg.de), [jure.zupan@cern.ch](mailto:jure.zupan@cern.ch)

## Abstract.

We present halo-independent methods to analyze the results of dark matter direct detection experiments assuming inelastic scattering. We focus on the annual modulation signal reported by DAMA/LIBRA and present three different halo-independent tests. First, we compare it to the upper limit on the unmodulated rate from XENON100 using (a) the trivial requirement that the amplitude of the annual modulation has to be smaller than the bound on the unmodulated rate, and (b) a bound on the annual modulation amplitude based on an expansion in the Earth's velocity. The third test uses the special predictions of the signal shape for inelastic scattering and allows for an internal consistency check of the data without referring to any astrophysics. We conclude that a strong conflict between DAMA/LIBRA and XENON100 in the framework of spin-independent inelastic scattering can be established independently of the local properties of the dark matter halo.

**Keywords:** dark matter theory, dark matter experiments

**ArXiv ePrint:** [1305.3575](https://arxiv.org/abs/1305.3575)

---

## Contents

|          |  |           |
|----------|--|-----------|
| <b>1</b> | <b>Introduction</b>  | <b>1</b>  |
| <b>2</b> | <b>Notation</b>  | <b>3</b>  |
| <b>3</b> | <b>Bound on the annual modulation amplitude from the expansion in <math>v_e</math></b> | <b>4</b>  |
| <b>4</b> | <b>Halo-independent tests for inelastic scattering</b>                                 | <b>7</b>  |
| <b>5</b> | <b>Conclusions</b>   | <b>11</b> |

---

## 1 Introduction

If dark matter (DM) is a “Weakly Interacting Massive Particle” (WIMP) it may induce an observable signal in underground detectors by depositing a tiny amount of energy after scattering with a nucleus in the detector material [1]. Many experiments are currently exploring this possibility and delivering a wealth of data. Among them is the DAMA/LIBRA experiment [2] (DAMA for short) which reports the striking signature of an annual modulation of the signal in their NaI scintillator detector, with a period of one year and a maximum around June 2nd with very high statistical significance. Such an effect is expected for DM induced events because the velocity of the detector relative to the DM halo changes due to the Earth’s rotation around the Sun [3, 4].

Assuming elastic spin-independent interactions the DAMA modulation signal is in strong tension with constraints on the total DM interaction rate from other experiments [5–8]. This problem can be alleviated by considering inelastic scattering [9], where the DM particle  $\chi$  up-scatters to an excited state  $\chi^*$  with a mass difference  $\delta = m_{\chi^*} - m_{\chi}$  comparable to the kinetic energy of the incoming particle, which is typically  $\mathcal{O}(100)$  keV. Under this hypothesis scattering off the heavy iodine nucleus is favoured compared to the relatively light sodium in the NaI crystal used in DAMA. Furthermore, the relative strength of the modulation signal compared to the unmodulated rate can be enhanced.<sup>1</sup> Nevertheless, under specific assumptions for the DM halo—typically a Maxwellian velocity distribution—also the inelastic scattering explanation of the DAMA signal is in tension with the bounds from XENON100 [12] and CRESST-II [10], see e.g., [13–16]. Below we show that this conclusion can be confirmed in a halo-independent way. Let us mention that any explanation of the DAMA signal based on iodine scattering is disfavoured also by KIMS results [17], since their 90% CL upper bound on the DM scattering rate on CsI is already somewhat lower than the size of the modulation amplitude observed in DAMA. This tension is completely independent of astrophysics as well as particle physics as long as scattering happens on iodine.

For typical inelastic scattering explanations of DAMA the mass splitting between the two DM states is chosen such that the minimal velocity,  $v_m$ , required to deposit the threshold

---

<sup>1</sup>The possibility to use inelastic scattering to reconcile the event excess observed in CRESST-II [10] with other bounds has been discussed in [11]. Here we do not follow this hypothesis and focus on the DAMA modulation signal.

energy in the detector is already close to the galactic escape velocity,  $v_{\text{esc}}$ . Only DM particles with velocities in the interval,  $v \in [v_{\text{esc}} - \Delta v, v_{\text{esc}}]$ , contribute, where  $\Delta v$  is the range of minimal velocities probed by the experiment and is comparable to the Earth’s velocity around the Sun,  $v_e \approx 30$  km/s. In this case the DM direct detection experiment probes the tails of the DM velocity distribution, where halo-substructures such as streams or debris flows are expected. The results are thus quite sensitive to the exact history of the Milky Way halo, mergers, etc, and significantly depend on the halo properties, see e.g. [18, 19]. Therefore it is important to develop astrophysics-independent methods to evaluate whether the above conclusion on the disagreement of the DAMA signal with other bounds is robust with respect to variations of DM halo properties.

An interesting method to compare signals and/or bounds from different experiments in an astrophysics independent way has been proposed in Refs. [20, 21]. This so-called  $v_m$ -method has been applied in various recent studies for elastic scattering, see e.g., [22–27]. The generalization of this method to inelastic scattering involves some complications which we are going to address in detail below.

In part of our analyses we will also use the fact that  $v_e$  is small compared to all other typical velocities in the problem. One can then derive astrophysics-independent bounds on the annual modulation signal [28] by expanding in  $v_e$  and relating the  $\mathcal{O}(v_e^0)$  and  $\mathcal{O}(v_e)$  terms in a halo-independent way. In [25, 28] the expansion was applied to the case of elastic DM scattering with DM masses of order 10 GeV, where the expansion is expected to be well-behaved, and it has been shown that for elastic scattering a strong tension between DAMA and constraints from other experiments can be established independent of the details of the DM halo. In the following we will generalize this type of analysis to the case of inelastic scattering, where special care has to be taken about whether the expansion in  $v_e$  remains well-behaved.

Below we will present three different tests for the consistency of the inelastic scattering interpretation of the DAMA signal, focusing on the tension with the bound from XENON100 [8]:

- the “trivial bound” obtained by the requirement that the amplitude of the annual modulation has to be smaller than the unmodulated rate,
- the bound on the annual modulation signal based on the expansion of the halo integral in  $v_e$ , and
- a test based on the predicted shape of the signal in the case of inelastic scattering which we call the “shape test” in the following.

The paper is structured as follows. We fix basic notation in Sec. 2. In Sec. 3 we discuss the bound on the annual modulation amplitude derived in [28]. By identifying the relevant expansion parameter we point out its limitations in the case of inelastic scattering. In Sec. 4 we develop halo-independent methods for inelastic scattering, focusing on the tension between DAMA and XENON100, and apply the three different types of tests mentioned above. Conclusions are presented in Sec. 5.

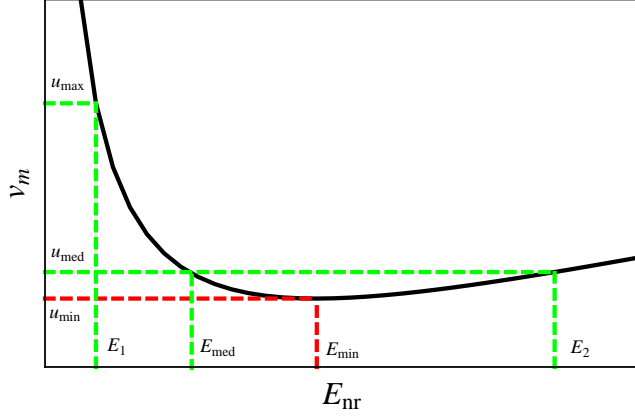


**Figure 1.**  $v_m$  as a function of  $E_{nr}$  for the case of inelastic scattering for some arbitrary  $\delta > 0$ .

## 2 Notation

The differential rate in events/keV/kg/day for DM  $\chi$  to scatter off a nucleus  $(A, Z)$  and deposit the nuclear recoil energy  $E_{nr}$  in the detector is

$$R(E_{nr}, t) = \frac{\rho_\chi}{m_\chi} \frac{1}{m_A} \int_{v > v_m} d^3v \frac{d\sigma_A}{dE_{nr}} v f_{\text{det}}(\mathbf{v}, t). \quad (2.1)$$

Here  $\rho_\chi \simeq 0.3 \text{ GeV/cm}^3$  is the local DM density,  $m_A$  and  $m_\chi$  are the nucleus and DM masses,  $\sigma_A$  the DM–nucleus scattering cross section and  $\mathbf{v}$  the 3-vector relative velocity between DM and the nucleus, while  $v \equiv |\mathbf{v}|$ . For a DM particle to deposit a recoil energy  $E_{nr}$  in the detector, a minimal velocity  $v_m$  is required, restricting the integral over velocities in Eq. (2.1). For inelastic scattering we have

$$v_m = \sqrt{\frac{1}{2m_A E_{nr}}} \left( \frac{m_A E_{nr}}{\mu_{\chi A}} + \delta \right), \quad (2.2)$$

where  $\mu_{\chi A}$  is the reduced mass of the DM–nucleus system, and  $\delta$  is the mass splitting between the two dark matter states. Note that for each value of  $E_{nr}$  there is a corresponding  $v_m$  while the converse is not always true. Certain values of  $v_m$  correspond to two values of  $E_{nr}$ , others maybe to none. This is illustrated in Fig. 1, where we plot  $v_m$  as a function of  $E_{nr}$  for some arbitrary  $\delta > 0$ .

The particle physics enters in Eq. (2.1) through the differential cross section. For the standard spin-independent and spin-dependent scattering the differential cross section is

$$\frac{d\sigma_A}{dE_{nr}} = \frac{m_A}{2\mu_{\chi A}^2 v^2} \sigma_A^0 F^2(E_{nr}), \quad (2.3)$$

where  $\sigma_A^0$  is the total DM–nucleus scattering cross section at zero momentum transfer, and  $F(E_{nr})$  is a form factor. We focus here on spin-independent inelastic scattering. We also assume that DM couples with the same strength to protons and neutrons ( $f_p = f_n$ ). Relaxing this assumption does not change the conclusions since DM particles scattering on Xe and I

have very similar dependence on  $f_n/f_p$  (cf. Fig. 5 of [11]). The astrophysics dependence enters in Eq. (2.1) through the DM velocity distribution  $f_{\text{det}}(\mathbf{v}, t)$  in the detector rest frame. Defining the halo integral

$$\eta(v_m, t) \equiv \int_{v > v_m} d^3v \frac{f_{\text{det}}(\mathbf{v}, t)}{v}, \quad (2.4)$$

the event rate is given by

$$R(E_{nr}, t) = C F^2(E_{nr}) \eta(v_m, t) \quad \text{with} \quad C = \frac{\rho_\chi \sigma_A^0}{2m_\chi \mu_{\chi A}^2}. \quad (2.5)$$

The coefficient  $C$  contains the particle physics dependence, while  $\eta(v_m, t)$  parametrizes the astrophysics dependence. The halo integral  $\eta(v_m, t)$  is the basis for the astrophysics independent comparison of experiments [20, 21] and we will make extensive use of it below.

### 3 Bound on the annual modulation amplitude from the expansion in $v_e$

In Ref. [28] some of us have derived an upper bound on the annual modulation amplitude in terms of the unmodulated rate. Here we briefly review the idea and generalize the bound to the case of inelastic scattering, where special care has to be taken about the validity of the expansion.

The DM velocity distribution in the rest frame of the Sun,  $f(\mathbf{v})$ , is related to the distribution in the detector rest frame by  $f_{\text{det}}(\mathbf{v}, t) = f(\mathbf{v} + \mathbf{v}_e(t))$ . The basic assumption of [28] is that  $f(\mathbf{v})$  is constant in time on the scale of 1 year and is constant in space on the scale of the size of the Sun–Earth distance. These are very weak requirements, called “Assumption 1” in [28], which are expected to hold for a wide range of possible DM halos. Those assumptions would be violated if a few DM substructures of  $\sim 1$  AU in size would dominate the local DM distribution. The smallest DM substructures in typical WIMP scenarios can have masses many orders of magnitude smaller than  $M_\odot$ , e.g. [29]. Based on numerical simulations it is estimated in [30] that Earth mass DM substructures with sizes comparable to the solar system are stable against gravitational disruption, and on average one of them will pass through the solar system every few thousand years, where such an encounter would last about 50 years. Those considerations suggest that Assumption 1 is well satisfied. Let us stress that typical DM streams or debris flows [31] which may dominate the DM halo at high velocities (especially relevant for inelastic scattering) are expected to be many orders of magnitude larger than 1 AU, and the relevant time scales are much larger than 1 yr, and hence they fulfill our assumptions, see e.g. [32] and references therein.

Under this assumption the only time dependence is due to the Earth’s velocity  $\mathbf{v}_e(t)$ , which we write as [33]

$$\mathbf{v}_e(t) = v_e[\mathbf{e}_1 \sin \lambda(t) - \mathbf{e}_2 \cos \lambda(t)], \quad (3.1)$$

with  $v_e = 29.8$  km/s, and  $\lambda(t) = 2\pi(t - 0.218)$  with  $t$  in units of 1 year and  $t = 0$  at January 1st, while  $\mathbf{e}_1 = (-0.0670, 0.4927, -0.8676)$  and  $\mathbf{e}_2 = (-0.9931, -0.1170, 0.01032)$  are orthogonal unit vectors spanning the plane of the Earth’s orbit which at this order can be assumed to be circular. The DM velocity distribution in the galactic frame is connected to the one in the rest frame of the Sun by  $f(\mathbf{v}) = f_{\text{gal}}(\mathbf{v} + \mathbf{v}_{\text{sun}})$ , with  $\mathbf{v}_{\text{sun}} \approx (0, 220, 0)$  km/s +  $\mathbf{v}_{\text{pec}}$  and  $\mathbf{v}_{\text{pec}} \approx (10, 13, 7)$  km/s the peculiar velocity of the Sun. We are using galactic coordinates

where  $x$  points towards the galactic center,  $y$  in the direction of the galactic rotation, and  $z$  towards the galactic north, perpendicular to the disc. As shown in [34], Eq. (3.1) provides an excellent approximation to describe the annual modulation signal.

Using the fact that  $v_e$  is small compared to other relevant velocities, one can expand the halo integral Eq. (2.4) in powers of  $v_e$ . At zeroth order one obtains

$$\eta_0(v_m) = \int_{v>v_m} d^3v \frac{f(\mathbf{v})}{v}, \quad (3.2)$$

which is responsible for the unmodulated (time averaged) rate up to terms of order  $v_e^2$ . The first order terms in  $v_e$  lead to the annual modulation signal, which due to Eq. (3.1) will have a pure sinusoidal shape, such that

$$\eta(v_m, t) = \eta_0(v_m) + A_\eta(v_m) \cos 2\pi[t - t_0(v_m)] + \mathcal{O}(v_e^2), \quad (3.3)$$

where the amplitude of the annual modulation,  $A_\eta(v_m)$ , is of first order in  $v_e$ .

In [28] it has been shown that under the above stated ‘‘Assumption 1’’ the modulation amplitude is bounded as

$$A_\eta(v_m) < v_e \left[ -\frac{d\eta_0}{dv_m} + \frac{\eta_0}{v_m} - \int_{v_m} dv \frac{\eta_0}{v^2} \right]. \quad (3.4)$$

From Eq. (3.2) it is clear that  $\eta_0$  is a positive decreasing function, i.e.,  $d\eta_0/dv_m < 0$ . As mentioned above, in the case of inelastic scattering typically only a small range in minimal velocities  $v_m$  is probed. We denote this interval by  $[u_{\min}, u_{\max}]$  with  $\Delta v = u_{\max} - u_{\min}$ . The boundaries of this interval are determined by the threshold of the detector on one side and by the galactic escape velocity or the nuclear form factor suppression on the other side. For inelastic scattering  $\Delta v$  is small. It will thus be convenient to integrate the inequality (3.4) over the interval  $[u_{\min}, u_{\max}]$ . By changing the order of integrations of the double integral we find

$$\begin{aligned} \int_{u_{\min}}^{u_{\max}} dv A_\eta(v) &< v_e \left[ \eta_0(u_{\min}) - \eta_0(u_{\max}) + u_{\min} \int_{u_{\min}}^{u_{\max}} dv \frac{\eta_0}{v^2} - \Delta v \int_{u_{\max}} dv \frac{\eta_0}{v^2} \right] \\ &< v_e \left[ \eta_0(u_{\min}) + u_{\min} \int_{u_{\min}}^{u_{\max}} dv \frac{\eta_0}{v^2} \right]. \end{aligned} \quad (3.5)$$

Integrating again over  $u_{\min}$  we obtain

$$\int_{u_{\min}}^{u_{\max}} dv A_\eta(v) (v - u_{\min}) < \frac{v_e}{2} \int_{u_{\min}}^{u_{\max}} dv \eta_0 \left( 3 - \frac{u_{\min}^2}{v^2} \right) \quad (3.6)$$

$$< \frac{v_e}{2} \left( 3 - \frac{u_{\min}^2}{u_{\max}^2} \right) \int_{u_{\min}}^{u_{\max}} dv \eta_0. \quad (3.7)$$

Hence we obtained a bound on the integral of the annual modulation in terms of an integral of the unmodulated rate at first order in  $v_e$ .<sup>2</sup> This bound receives no corrections at order

---

<sup>2</sup>Below we will use the bound (3.7) for the numerical analysis since this will allow for easy comparison with the ‘‘trivial bound’’ discussed later. The numerical difference between the bounds using (3.7) or (3.6) is small, typically less than 10%.

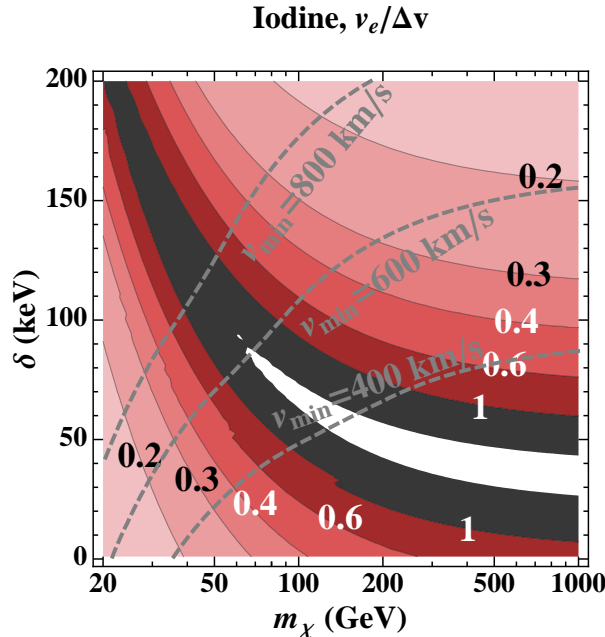


**Figure 2.** Contours of the ratio  $v_e/\Delta v$  as a function of DM mass  $m_\chi$  and mass splitting  $\delta$  for scattering on iodine in DAMA, assuming that  $\Delta v$  is the overlap between the velocity ranges corresponding to the DAMA [2, 4] keVee energy range for scattering on iodine and the XENON100 [6.61, 43.04] keV range. Dashed curves show contours of constant  $v_m = 400, 600, 800$  km/s, with  $v_m$  being the minimal velocity corresponding to the above energy interval for the given  $\delta$  and  $m_\chi$ .

$\mathcal{O}(v_e^2)$  and hence is valid up to (but not including) terms of order  $\mathcal{O}(v_e^3)$  [35]. In applying Eq. (3.7) we use only an upper bound,  $\eta_{\text{bnd}}$  on the unmodulated signal  $\eta_0$ , allowing also for the presence of background. However, we assume that  $A_\eta$  is background free, i.e., the background shows no annual modulation.

Let us define the average over the velocity interval by

$$\langle X \rangle = \frac{1}{\Delta v} \int_{u_{\min}}^{u_{\max}} dv X(v). \quad (3.8)$$

Estimating  $\int_{u_{\min}}^{u_{\max}} dv A_\eta(v)(v - u_{\min}) \sim \Delta v \int_{u_{\min}}^{u_{\max}} dv A_\eta(v)$  and neglecting  $\mathcal{O}(1)$  coefficients we obtain from Eq. (3.7)

$$\langle A_\eta \rangle \lesssim \frac{v_e}{\Delta v} \langle \eta_0 \rangle. \quad (3.9)$$

This shows that the expansion parameter in deriving the bound (3.7) is  $v_e/\Delta v$ . In contrast to expressions like  $v_e/u_{\min}$  which are always small, the ratio  $v_e/\Delta v$  can become of order one, in particular for inelastic scattering.

As an example we show in Fig. 2 the ratio  $v_e/\Delta v$  as a function of the DM mass  $m_\chi$  and the inelasticity parameter  $\delta$ . Elastic scattering is recovered for  $\delta = 0$ . The velocity interval  $\Delta v$  is chosen having in mind a possible explanation for DAMA. The signal in DAMA is predominantly in the energy region [2, 4] keVee. As explained in Section 4 below, we take for  $\Delta v$  the overlap between the velocity ranges corresponding to the DAMA [2, 4] keVee interval for scattering on iodine and the XENON100 [6.61, 43.04] keV interval. From Fig. 2 one sees

that the expansion parameter  $v_e/\Delta v \gtrsim 1$  for a non-negligible part of the parameter space of DM masses  $m_\chi$  and mass splittings  $\delta$ . For those values of  $m_\chi$  and  $\delta$  the bound Eq. (3.7) does not apply. Still, in a significant part of the parameter space  $v_e/\Delta v$  is sufficiently small such that the expansion can be performed. In particular, we observe from the figure that for elastic scattering ( $\delta = 0$ ) and  $m_\chi \lesssim 50$  the expansion parameter is small, justifying the approach of Ref. [25].

#### 4 Halo-independent tests for inelastic scattering

In this section we present three different halo-independent tests of the tension between the DAMA annual modulation signal [2] and the bound from XENON100 [8] in the framework of inelastic scattering. The tests are presented in the following order. First, we present the shape test which is a test based on the predicted shape of the signal. Second, we present the bound on the annual modulation signal from Eq. (3.7). Third, we present the trivial bound which is based on the fact that the amplitude of the annual modulation must be smaller than the unmodulated rate.

The  $v_m$  method [20, 21] to compare different experiments like DAMA and XENON100 requires to translate the physical observations in nuclear recoil energy  $E_{nr}$  into  $v_m$  space using Eq. (2.2). Then experiments can be directly compared based on the halo integral  $\eta(v_m)$  or inequalities such as Eq. (3.7) [25]. However, for inelastic scattering this involves some complications. The reason is that in inelastic scattering each minimal velocity  $v_m$  can correspond to up to two values of  $E_{nr}$ , depending on the values of  $m_\chi$  and  $\delta$ . This has to be taken into account when translating an observation at a given  $E_{nr}$  into  $v_m$ , since the relation between them is no longer unique (as it is for elastic scattering). Solving Eq. (2.2) for  $E_{nr}$ , one obtains two solutions  $E_\pm$  as a function of  $v_m$ ,

$$E_\pm = \left( \frac{\mu_{\chi A}}{m_A} \right) \left[ (\mu_{\chi A} v_m^2 - \delta) \pm v_m \sqrt{\mu_{\chi A} (\mu_{\chi A} v_m^2 - 2\delta)} \right]. \quad (4.1)$$

There is a minimal value of  $v_m$  given by  $\sqrt{2\delta/\mu_{\chi A}}$  at an energy  $E_{\min} = \mu_{\chi A} \delta / M_A$ .

Let us consider the following situation, having in mind DAMA: we have a region  $[E_1, E_2]$  in nuclear recoil energy where the modulation amplitude is non-zero. We assume that  $E_1$  is the threshold energy of the detector. When mapped into  $v_m$  space according to Eq. (2.2) we obtain that the whole interval  $[E_1, E_2]$  is mapped into a small region in  $v_m$ , between  $u_{\min}$  and  $u_{\max}$  with  $u_{\max} - u_{\min} \ll u_{\min}$ , where  $u_{\min}$  and  $u_{\max}$  are the minimum and maximum values of  $v_m$  in the  $[E_1, E_2]$  interval, respectively. For the special case plotted in Fig. 1,  $u_{\min} = v_m(E_{\min})$ , and  $u_{\max} = v_m(E_1)$ . In general, depending on the shape of  $v_m$  as a function of  $E_{nr}$  in the interval  $[E_1, E_2]$ ,  $u_{\max}$  may either be  $v_m(E_1)$  (as in the case shown in Fig. 1) or  $v_m(E_2)$ . Furthermore, in cases where  $E_{\min}$  falls outside of the interval  $[E_1, E_2]$ ,  $u_{\min}$  will either be  $v_m(E_1)$  or  $v_m(E_2)$ . We will not discuss all these cases here explicitly, but as an example focus on the case shown in Fig. 1.

To compute the bound in Eq. (3.7) using DAMA data, we need to numerically compute integrals such as  $\int_{u_{\min}}^{u_{\max}} dv h(v) A_\eta^{\text{obs}}(v)$  where  $h(v) = v - u_{\min}$  is specified in Eq. (3.7) (we leave it general here to apply the same formalism also to the bound in Eq. (4.7) discussed later on, where  $h(v) = 1$ ) and  $A_\eta^{\text{obs}}(v)$  is the observed amplitude of the annual modulation in units of events/kg/day/keV. In order to compute those integrals we have to consider the functional

relation between  $v_m$  and  $E_{nr}$  in the relevant interval  $[E_1, E_2]$ . Let us discuss for instance the situation depicted in Fig. 1. In this case we have

$$\begin{aligned} \int_{u_{\min}}^{u_{\max}} dv h(v) \tilde{A}_\eta^{\text{obs}}(v) &= \int_{u_{\min}}^{u_{\text{med}}} dv h(v) \tilde{A}_\eta^{\text{obs}}(v) + \int_{u_{\text{med}}}^{u_{\max}} dv h(v) \tilde{A}_\eta^{\text{obs}}(v) \\ &= \int_{u_{\min}}^{u_{\text{med}}} dv h(v) \tilde{A}_\eta^{\text{obs}}(v) + \int_{E_{\text{med}}}^{E_1} dE_{nr} \frac{dv}{dE_{nr}} h(E_{nr}) \tilde{A}_\eta^{\text{obs}}(v). \end{aligned} \quad (4.2)$$

Here,  $u_{\text{med}} = v_m(E_2)$  and  $E_{\text{med}} = E_-(u_{\text{med}})$ . The integrals can be written as a sum of several integrals which are evaluated over energy bins, as given by the DAMA binning. We take four bins of equal size in the [2, 4] keVee range for the DAMA data. In each bin we write [25]

$$\tilde{A}_\eta^{\text{obs}}(v_i) = \frac{A_i^{\text{obs}} q_I}{A_I^2 F_I^2(E_{nr}) f_I}, \quad (4.3)$$

where the index  $i$  labels energy bins,  $q_I$  is the iodine quenching factor for which we take  $q_I = 0.09^3$ ,  $F_I(E_{nr})$  is the Helm form factor for iodine, and  $f_I = m_I/(m_{\text{Na}} + m_I)$ . In each energy bin we assume  $A_i^{\text{obs}}$  is constant, and thus in each bin we numerically integrate  $(dv/dE_{nr})h(E_{nr})/F_I^2(E_{nr})$  over the bin width.

For the first integral on the r.h.s. of Eq. (4.2) there is an ambiguity, since the interval  $[u_{\min}, u_{\text{med}}]$  corresponds to two regions in energy:  $[E_{\text{med}}, E_{\min}]$  or  $[E_{\min}, E_2]$ . If the inelastic DM hypothesis under consideration is correct, both energy intervals should give the same value of the integral. We can use this observation to test the hypothesis that the signal is due to inelastic DM scattering by requiring that the two integrals agree within experimental errors. In the following, we will call this the ‘‘shape test’’. Let us denote the integrals corresponding to the two energy intervals by  $I_a$  and  $I_b$  and their experimental errors by  $\sigma_a$  and  $\sigma_b$ , correspondingly. In Fig. 3 we show the difference weighted by the error as obtained from DAMA data:

$$\frac{|I_a - I_b|}{\sqrt{\sigma_a^2 + \sigma_b^2}}. \quad (4.4)$$

We observe that a strip in the parameter space in  $\delta$  and  $m_\chi$  is already excluded by this requirement at more than  $3\sigma$  in a completely halo-independent way, just requiring a spectral shape of the signal consistent with the inelastic scattering hypothesis. In cases where the two values are consistent within errors we use for the integral the weighted average of the two values. In Fig. 3,  $I_a$  and  $I_b$  are evaluated for the choice of  $h(v) = v - u_{\min}$ . The shape test is only slightly different for  $h(v) = 1$  which is the case for the trivial bound explained later in Eq. (4.7).

In order to evaluate the r.h.s. of the inequality in Eq. (3.7), we need to calculate an integral over the experimental upper bound  $\tilde{\eta}_{\text{bnd}}(v_m)$  on the unmodulated signal, with

$$\tilde{\eta}(v_m) \equiv \frac{\sigma_p \rho_\chi}{2m_\chi \mu_{\chi p}^2} \eta_0(v_m), \quad (4.5)$$

where  $\sigma_p$  is the cross section on a nucleon and  $\mu_{\chi p}$  is the DM–nucleon reduced mass.  $\tilde{\eta}$  has units of events/kg/day/keV. In using Eqs. (4.3) and (4.5) we have assumed an  $A^2$  dependence

<sup>3</sup>For DM masses that we consider one can safely neglect scattering on sodium. Note also that the channeling fraction of iodine in NaI is likely to be very small and can be neglected [36].

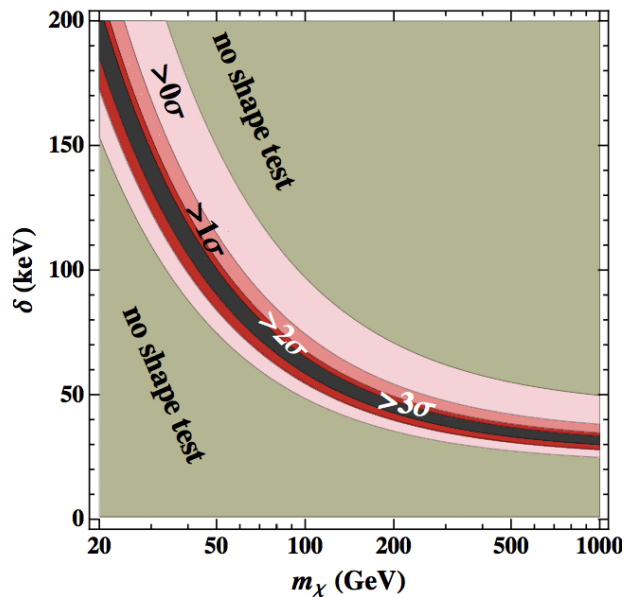


**Figure 3.** The DM exclusion regions (red bands, with significance as denoted) that follow from the internal consistency shape test for DAMA data, see Eq. (4.4). In the gray region denoted by “no shape test” there is a one-to-one correspondence between  $E_{nr}$  and  $v_m$  since  $E_{\min}$  lies outside the relevant energy interval  $[E_1, E_2]$  and therefore the shape test cannot be applied.

of the scattering cross section on the nucleus with mass number  $A$ . We use the method discussed in Ref. [25] (see also [20]) to evaluate  $\tilde{\eta}_{\text{bnd}}(v_m)$  for the inelastic case. Namely, we use the fact that  $\tilde{\eta}(v_m)$  is a falling function, and that the minimal number of events is obtained for  $\tilde{\eta}$  constant and equal to  $\tilde{\eta}(v_m)$  up to  $v_m$  and zero for larger values of  $v_m$ . Therefore, for a given  $v_m$  we have a lower bound on the predicted number of events in an interval of observed energies  $[E_1, E_2]$ ,  $N_{[E_1, E_2]}^{\text{pred}} > \mu(v_m)$  with

$$\mu(v_m) = MTA^2\tilde{\eta}(v_m) \int_{E_-}^{E_+} dE_{nr} F_A^2(E_{nr}) G_{[E_1, E_2]}(E_{nr}), \quad (4.6)$$

where  $G_{[E_1, E_2]}(E_{nr})$  is the detector response function which describes the contribution of events with the nuclear-recoil energy  $E_{nr}$  to the observed energy interval  $[E_1, E_2]$ .  $M$  and  $T$  are the detector mass and exposure time, respectively. Notice that  $\mu(v_m)$  for the elastic case is given in Eq. (10) of Ref. [25] and in that case the integral is computed between 0 and  $E(v_m)$  which corresponds to velocities below a fixed  $v_m$ . For the inelastic case, we have two solutions  $E_+$  and  $E_-$  for each  $v_m$ , and the region in velocity space below  $v_m$  is precisely, the region  $E_- < E_{nr} < E_+$ .

Assuming an experiment observes  $N_{[E_1, E_2]}^{\text{obs}}$  events in the interval  $[E_1, E_2]$ , we can obtain an upper bound on  $\tilde{\eta}(v_m)$  for a fixed  $v_m$  at a confidence level CL by requiring that the probability of obtaining  $N_{[E_1, E_2]}^{\text{obs}}$  events or less for a Poisson mean of  $\mu(v_m)$  is equal to  $1 - \text{CL}$ . The upper bound obtained in this way is  $\tilde{\eta}_{\text{bnd}}(v_m)$  and can then be used in Eq. (3.7) and numerically integrated over  $[u_{\min}, u_{\max}]$  to constrain the modulation amplitude. We use the data from XENON100 [8] where the  $E_{nr}$  interval [6.61, 43.04] keV is binned into four bins. In

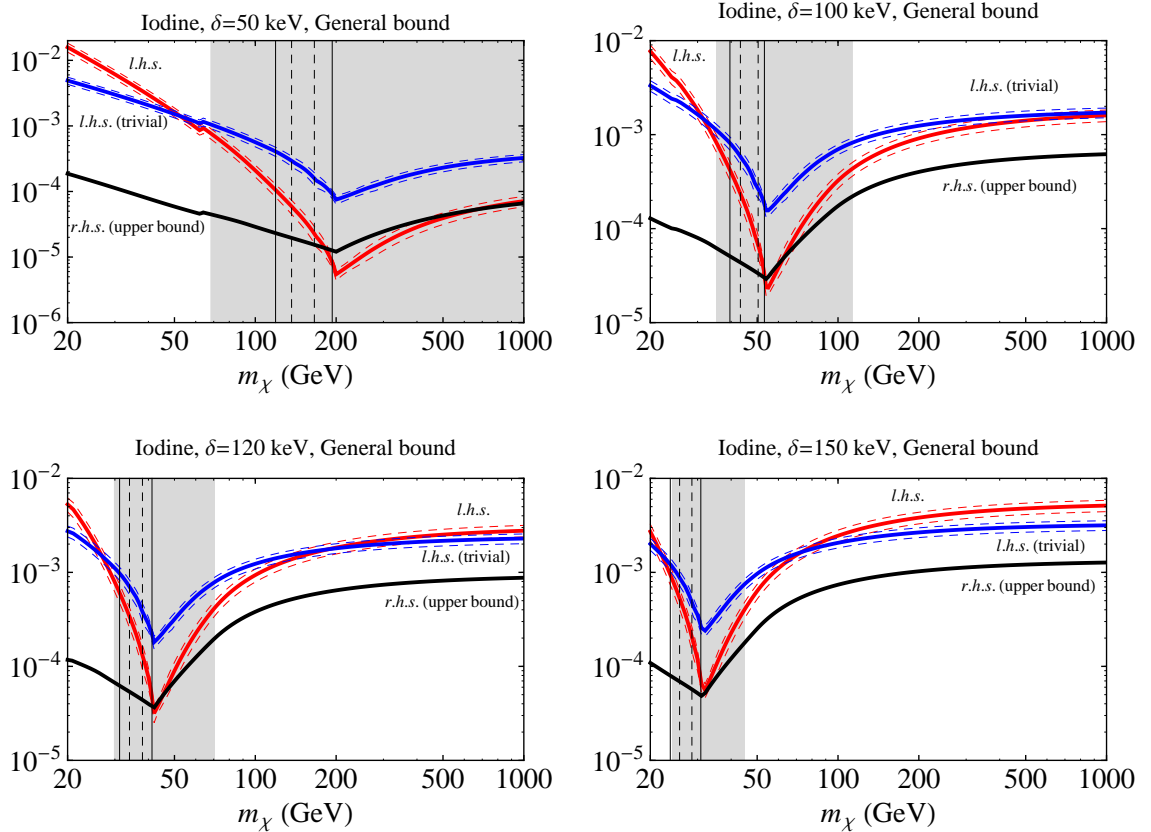


**Figure 4.** The bounds from Eqs. (3.7) and (4.7) for DAMA data as a function of  $m_\chi$  for  $\delta = 50, 100, 120, 150$  keV. The red curve labeled “l.h.s.” shows the integral on the l.h.s. of Eq. (3.7), whereas the blue curve labeled “l.h.s. (trivial)” corresponds to the l.h.s. of the trivial bound in Eq. (4.7). The dashed curves indicate the  $1\sigma$  error. The black curve labeled “r.h.s. (upper bound)” is the same for (3.7) and (4.7) and has been obtained from the  $3\sigma$  limit on  $\eta_{\text{bnd}}$  from XENON100 data. The units on the vertical axis are counts/kg/day/keV (km/s)<sup>2</sup>. In the gray shaded regions we have  $v_e/\Delta v > 0.7$ ; truncating the expansion may not be a good approximation and hence, the red curve should not be trusted in those regions, but instead the blue one can be used there. The solid (dashed) vertical lines indicate the regions where the two integrals relevant for the “shape test” differ by more than  $2\sigma$  ( $3\sigma$ ) according to Eq. (4.4).

each bin we calculate the probability of obtaining  $N_{[E_1, E_2]}^{\text{obs}}$  events or less for a Poisson mean of  $\mu(v_m)$  as described above, and then multiply the probability of the four bins to obtain the overall probability, giving finally the actually observed event distribution. Note, that since only the high energy range in Xenon is relevant, our results are not sensitive to uncertainties in the scintillation efficiency  $\mathcal{L}_{\text{eff}}$  at low energies. For the comparison of the DAMA and XENON100 data using Eq. (3.7) we define the  $[u_{\text{min}}, u_{\text{max}}]$  range as the overlap between  $v_m$  spaces corresponding to the DAMA iodine [2, 4] keVee range and the XENON100 [6.61, 43.04] keV range.<sup>4</sup>

In Fig. 4 we show the l.h.s. and r.h.s. of the bound from Eq. (3.7) in red and black,

<sup>4</sup>For most of the region in parameter space this joint interval is actually very close to the one coming from DAMA iodine [2, 4] keVee.

respectively, as a function of  $m_\chi$  for  $\delta = 50$  keV, 100 keV, 120 keV, and 150 keV. We calculate the integral over the annual modulation amplitude in the l.h.s. of Eq. (3.7) as described above. The red dashed curves indicate the  $1\sigma$  error on the integral. The upper limit on the r.h.s. of Eq. (3.7) is calculated from the XENON100  $3\sigma$  upper limit. We see that in most regions of the parameter space the bound is strongly violated, disfavoring an inelastic scattering interpretation of the DAMA signal halo-independently. Note that DM mass enters only via  $\mu_{\chi A}$ , so that  $\mu_{\chi A} \simeq m_A$  for  $m_\chi \gg m_A$ , and Eq. (4.1) becomes independent of  $m_\chi$ . This is what we see in Fig. 4, where curves become flat for large  $m_\chi$  and therefore the tension between XENON100 and DAMA cannot be diminished when going to larger DM masses.

The shaded regions in Fig. 4 are the regions where the expansion parameter  $v_e/\Delta v$  is large (we take somewhat arbitrarily  $v_e/\Delta v > 0.7$ , cf. also Fig. 2). Hence, in the shaded regions the astrophysics independent bound on the modulation amplitude, Eq. (3.7) (the red curves in Fig. 4), can receive  $\mathcal{O}(1)$  corrections and should not be trusted. Interestingly, however, part of the region where the  $v_e$  expansion breaks down is disfavored by the internal consistency “shape test”, Eq. (4.4). We indicate the range in  $m_\chi$  where the two integrals differ by more than  $2\sigma$  and  $3\sigma$  with vertical lines, cf. also Fig. 3.

Finally we consider the “trivial bound”, which is based on the simple fact valid for any positive function that the amplitude of the first harmonic has to be smaller than the constant part, i.e.,  $A_\eta \leq \eta_0$ . To compare directly with Eq. (3.7), we can write the trivial bound as,

$$\frac{v_e}{2} \left( 3 - \frac{u_{\min}^2}{u_{\max}^2} \right) \int_{u_{\min}}^{u_{\max}} dv A_\eta(v) < \frac{v_e}{2} \left( 3 - \frac{u_{\min}^2}{u_{\max}^2} \right) \int_{u_{\min}}^{u_{\max}} dv \eta_{\text{bnd}}(v). \quad (4.7)$$

The l.h.s. of this relation is shown as blue curve in Fig. 4 together with its  $1\sigma$  error band. We observe again strong tension with the upper bound from XENON100 data. Clearly this bound is independent of any expansion parameter and is valid in the full parameter space. In the regions where the expansion is expected to break down (i.e., the grey shaded regions) this bound can be used to exclude the inelastic explanation for DAMA. From Fig. 4 we also observe that in the regions where the expansion in  $v_e$  is expected to be valid the modulation bound from Eq. (3.7) becomes stronger (or at least comparable – for large  $m_\chi$ ) to the trivial bound.

## 5 Conclusions

Inelastic scattering [9] has originally been invoked to reconcile the DAMA annual modulation signal with bounds from other experiments. Using the kinematics of inelastic scattering the annual modulation amplitude can be enhanced compared to the time averaged rate. This is achieved at the expense of tuning the minimal velocity probed by the experiment so that it is close to the galactic escape velocity, which makes the signal rather sensitive to properties of the tails of the dark matter velocity distribution. Hence it is important to establish halo-independent methods for this scenario.

In this work we have generalized the comparison of dark matter direct detection experiments in  $v_m$  space [20, 21] to the case of inelastic scattering. This is non-trivial due to the non-unique relation between the recoil energy and  $v_m$ . Turning this complication into a virtue, we presented a consistency check based on the particular shape of the signal for

inelastic scattering which we dubbed the “shape test”, given in Eq. (4.4) and Fig. 3. In certain regions of the parameter space the inelastic scattering hypothesis can be excluded simply based on the energy spectrum of the modulation signal, without referring to halo properties.

Furthermore, we have applied a bound on the annual modulation amplitude based on an expansion of the halo integral in the Earth’s velocity  $v_e$  [28]. We have identified the relevant expansion parameter to be  $v_e/\Delta v$ , where  $\Delta v$  is the range in minimal velocities  $v_m$  probed in the experiment. For inelastic scattering,  $\Delta v$  can become of order  $v_e$  for part of the  $(m_\chi, \delta)$  parameter space, and then the bound cannot be applied. However, in those cases one can use the “trivial bound”, requiring that the amplitude of the annual modulation has to be less than the bound on the unmodulated rate.

We were able to show that XENON100 strongly disfavors an interpretation of the DAMA modulation signal in terms of inelastic scattering, independent of assumptions on the properties of the local dark matter velocity distribution. Beyond the immediate problem of interpreting the DAMA signal, the methods developed in this manuscript will provide a valuable consistency check for an inelastic scattering interpretation of any future dark matter signal.

In our work we have focused on spin-independent contact interactions, where the differential scattering cross section takes the form of Eq. (2.3). Our considerations generalize trivially to other interaction types which lead to a similar  $1/v^2$  dependence (e.g., the spin-dependent inelastic scattering considered in [15]) but may feature a different dependence on  $E_{nr}$ . Furthermore, the shape test and the trivial bound can be applied for any particle physics model where the differential cross section factorizes as  $X(v)Y(E_{nr})$ , where  $X$  and  $Y$  are arbitrary functions of  $v$  and  $E_{nr}$ , respectively. An example where such a factorization is not possible in general are magnetic interactions, e.g. [37]. In such cases generalized methods as presented recently in [38] may be invoked.

## Acknowledgements

N.B., J.H.-G., and T.S. acknowledge support from the European Union FP7 ITN INVISIBLES (Marie Curie Actions, PITN-GA-2011-289442). J.H.-G. is supported by the MICINN under the FPU program. J.Z. was supported in part by the U.S. National Science Foundation under CAREER Grant PHY-1151392.

## References

- [1] M. W. Goodman and E. Witten, *Detectability of Certain Dark Matter Candidates*, Phys.Rev. **D31**, 3059 (1985).
- [2] DAMA/LIBRA Collaboration, R. Bernabei *et al.*, *New results from DAMA/LIBRA*, Eur.Phys.J. **C67**, 39 (2010), 1002.1028.
- [3] A. K. Drukier, K. Freese, and D. N. Spergel, *Detecting Cold Dark Matter Candidates*, Phys. Rev. **D33**, 3495 (1986).
- [4] K. Freese, J. A. Frieman, and A. Gould, *Signal Modulation in Cold Dark Matter Detection*, Phys. Rev. **D37**, 3388 (1988).
- [5] CDMS-II Collaboration, Z. Ahmed *et al.*, *Dark Matter Search Results from the CDMS II Experiment*, Science **327**, 1619 (2010), 0912.3592.

- [6] CDMS-II, Z. Ahmed *et al.*, *Results from a Low-Energy Analysis of the CDMS II Germanium Data*, Phys. Rev. Lett. **106**, 131302 (2011), 1011.2482.
- [7] XENON10 Collaboration, J. Angle *et al.*, *A search for light dark matter in XENON10 data*, Phys.Rev.Lett. **107**, 051301 (2011), 1104.3088.
- [8] XENON100 Collaboration, E. Aprile *et al.*, *Dark Matter Results from 225 Live Days of XENON100 Data*, Phys.Rev.Lett. **109**, 181301 (2012), 1207.5988.
- [9] D. Tucker-Smith and N. Weiner, *Inelastic dark matter*, Phys. Rev. **D64**, 043502 (2001), hep-ph/0101138.
- [10] G. Angloher *et al.*, *Results from 730 kg days of the CRESST-II Dark Matter Search*, Eur.Phys.J. **C72**, 1971 (2012), 1109.0702.
- [11] J. Kopp, T. Schwetz, and J. Zupan, *Light Dark Matter in the light of CRESST-II*, JCAP **1203**, 001 (2012), 1110.2721.
- [12] XENON100 Collaboration, E. Aprile *et al.*, *Implications on Inelastic Dark Matter from 100 Live Days of XENON100 Data*, Phys.Rev. **D84**, 061101 (2011), 1104.3121.
- [13] S. Chang, G. D. Kribs, D. Tucker-Smith, and N. Weiner, *Inelastic Dark Matter in Light of DAMA/LIBRA*, Phys.Rev. **D79**, 043513 (2009), 0807.2250.
- [14] K. Schmidt-Hoberg and M. W. Winkler, *Improved Constraints on Inelastic Dark Matter*, JCAP **0909**, 010 (2009), 0907.3940.
- [15] J. Kopp, T. Schwetz, and J. Zupan, *Global interpretation of direct Dark Matter searches after CDMS-II results*, JCAP **1002**, 014 (2010), 0912.4264.
- [16] C. Arina, *Chasing a consistent picture for dark matter direct searches*, Phys.Rev. **D86**, 123527 (2012), 1210.4011.
- [17] S. Kim *et al.*, *New Limits on Interactions between Weakly Interacting Massive Particles and Nucleons Obtained with CsI(Tl) Crystal Detectors*, Phys.Rev.Lett. **108**, 181301 (2012), 1204.2646.
- [18] J. March-Russell, C. McCabe, and M. McCullough, *Inelastic Dark Matter, Non-Standard Halos and the DAMA/LIBRA Results*, JHEP **0905**, 071 (2009), 0812.1931.
- [19] M. Lisanti, L. E. Strigari, J. G. Wacker, and R. H. Wechsler, *The Dark Matter at the End of the Galaxy*, Phys.Rev. **D83**, 023519 (2011), 1010.4300.
- [20] P. J. Fox, J. Liu, and N. Weiner, *Integrating Out Astrophysical Uncertainties*, Phys.Rev. **D83**, 103514 (2011), 1011.1915.
- [21] P. J. Fox, G. D. Kribs, and T. M. Tait, *Interpreting Dark Matter Direct Detection Independently of the Local Velocity and Density Distribution*, Phys.Rev. **D83**, 034007 (2011), 1011.1910.
- [22] C. McCabe, *DAMA and CoGeNT without astrophysical uncertainties*, Phys.Rev. **D84**, 043525 (2011), 1107.0741.
- [23] M. T. Frandsen, F. Kahlhoefer, C. McCabe, S. Sarkar, and K. Schmidt-Hoberg, *Resolving astrophysical uncertainties in dark matter direct detection*, JCAP **1201**, 024 (2012), 1111.0292.
- [24] P. Gondolo and G. B. Gelmini, *Halo independent comparison of direct dark matter detection data*, JCAP **1212**, 015 (2012), 1202.6359.
- [25] J. Herrero-Garcia, T. Schwetz, and J. Zupan, *Astrophysics independent bounds on the annual modulation of dark matter signals*, Phys.Rev.Lett. **109**, 141301 (2012), 1205.0134.
- [26] M. T. Frandsen, F. Kahlhoefer, C. McCabe, S. Sarkar, and K. Schmidt-Hoberg, *The unbearable*

- lightness of being: CDMS versus XENON*, (2013), 1304.6066.
- [27] E. Del Nobile, G. B. Gelmini, P. Gondolo, and J.-H. Huh, *Halo-independent analysis of direct detection data for light WIMPs*, (2013), 1304.6183.
  - [28] J. Herrero-Garcia, T. Schwetz, and J. Zupan, *On the annual modulation signal in dark matter direct detection*, JCAP **1203**, 005 (2012), 1112.1627.
  - [29] T. Bringmann, *Particle Models and the Small-Scale Structure of Dark Matter*, New J.Phys. **11**, 105027 (2009), 0903.0189.
  - [30] J. Diemand, B. Moore, and J. Stadel, *Earth-mass dark-matter haloes as the first structures in the early Universe*, Nature **433**, 389 (2005), astro-ph/0501589.
  - [31] M. Kuhlen, M. Lisanti, and D. N. Spergel, *Direct Detection of Dark Matter Debris Flows*, Phys.Rev. **D86**, 063505 (2012), 1202.0007.
  - [32] K. Freese, M. Lisanti, and C. Savage, *Annual Modulation of Dark Matter: A Review*, (2012), 1209.3339.
  - [33] G. Gelmini and P. Gondolo, *WIMP annual modulation with opposite phase in Late-Infall halo models*, Phys.Rev. **D64**, 023504 (2001), hep-ph/0012315.
  - [34] A. M. Green, *Effect of realistic astrophysical inputs on the phase and shape of the WIMP annual modulation signal*, Phys. Rev. **D68**, 023004 (2003), astro-ph/0304446.
  - [35] N. Bozorgnia, J. Herrero-Garcia, T. Schwetz, and J. Zupan, *in preparation*, (2013).
  - [36] N. Bozorgnia, G. B. Gelmini, and P. Gondolo, *Channeling in direct dark matter detection I: channeling fraction in NaI (Tl) crystals*, JCAP **1011**, 019 (2010), 1006.3110.
  - [37] S. Chang, N. Weiner, and I. Yavin, *Magnetic Inelastic Dark Matter*, Phys. Rev. **D82**, 125011 (2010), 1007.4200.
  - [38] E. Del Nobile, G. Gelmini, P. Gondolo, and J.-H. Huh, *Generalized Halo Independent Comparison of Direct Dark Matter Detection Data*, (2013), 1306.5273.